
Partly Supervised Multitask Learning

Abdullah-Al-Zubaer Imran^{1,2} Chao Huang² Hui Tang² Wei Fan²
Yuan Xiao³ Dingjun Hao³ Zhen Qian² Demetri Terzopoulos^{1,4}

Abstract

Semi-supervised learning has recently been attracting attention as an alternative to fully supervised models that require large pools of labeled data. Moreover, optimizing a model for multiple tasks can provide better generalizability than single-task learning. Leveraging self-supervision and adversarial training, we propose a novel general purpose semi-supervised, multiple-task model—namely, self-supervised, semi-supervised, multitask learning (S⁴MTL)—for accomplishing two important tasks in medical imaging, segmentation and diagnostic classification. Experimental results on chest and spine X-ray datasets suggest that our S⁴MTL model significantly outperforms semi-supervised single task, semi/fully-supervised multitask, and fully-supervised single task models, even with a 50% reduction of class and segmentation labels. We hypothesize that our proposed model can be effective in tackling limited annotation problems for joint training, not only in medical imaging domains, but also for general-purpose vision tasks.

1. Introduction

The success of fully-supervised deep convolutional neural networks (CNNs) currently relies on large quantities of labeled data. However, in certain applications such as medical imaging, such annotated data are often either unavailable or expensive and time-consuming to obtain. Therefore, for real-world applications, there is growing interest in leveraging limited quantities of labeled data along with much greater quantities of unlabeled data. Such approaches are called semi-supervised learning (SSL). For them to be effective, however, the knowledge gained from the unlabeled data must be significant to the model (Chapelle et al., 2009).

¹Department of Computer Science, University of California, Los Angeles, California, USA ²Tencent Hippocrates Research Lab, Palo Alto, California, USA ³Xian Jiaotong University College of Medicine, China ⁴VoxelCloud, Inc., Los Angeles, California, USA. Correspondence to: Abdullah-Al-Zubaer Imran <aimran@cs.ucla.edu>.

Depending on how unlabeled data are leveraged, semi-supervised learning can be accomplished in several ways, and this has recently emerged as a growing body of research, yielding schemes such as unsupervised domain adaptation (Zhang et al., 2019), self-supervised learning (Jing & Tian, 2019), adversarial learning (Donahue et al., 2016), and multitask learning (Ruder, 2017). In unsupervised domain adaptation, a model is pre-trained on similar tasks in some other domains with labeled data, and the pre-trained model is then fine-tuned with a limited set of labeled data in the target domain. Domain adaption can also be performed to learn a generic representation where the model is fully-supervised for source data and unsupervised for the target data (Yang et al., 2019; Zhuang et al., 2019). Self-supervised learning is closely related to transfer learning. Unlike transfer learning, the model is pre-trained on some surrogate tasks in the same domain, and then the pre-trained model is evaluated on the main application tasks in computer vision or medical imaging. Self-supervised learning is usually based on the assumption that the predicted labels from the original data and the augmented data should be the same (Jing & Tian, 2019). Adversarial learning, like Generative Adversarial Networks (GANs) (Goodfellow et al., 2014), augments the class labels with an additional label to differentiate the generated data and real data. A well balanced generator-discriminator helps towards learning useful visual features from the unlabeled data (Donahue et al., 2016). Multitask learning (MTL) is basically defined as optimizing more than one loss. In MTL, multiple related tasks are jointly learned, which results in better generalization of the model (Ruder, 2017). Moreover, jointly learning multiple tasks as a general objective improves performance compared to single-task learning (Zhang & Yang, 2017).

We propose a self-supervised, semi-supervised, multitask learning (S⁴MTL) model that combines the advantages of self-supervised learning, adversarial learning, and multitask learning for real applications. Unlike simply optimizing multiple losses in the model, multiple real tasks are accomplished in our proposed approach. To demonstrate its effectiveness, our S⁴MTL model is applied to two of the most important tasks in medical imaging—segmentation of anatomical structures and diagnostic classification—and both tasks are tackled by the same model. Clinically, it is important to label an image as normal or abnormal, but also

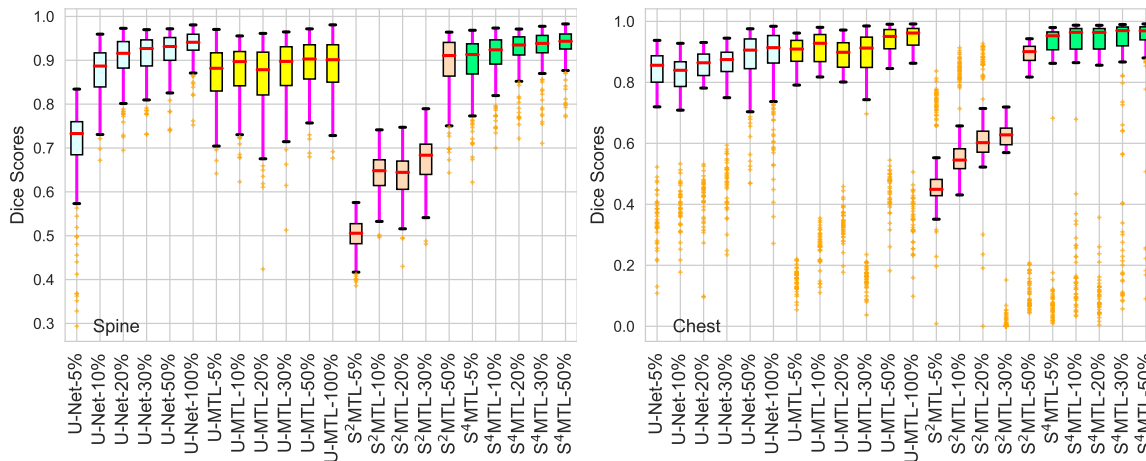


Figure 1. Box-Whisker plots showing consistent improvement in segmentation performance by the S^4 MTL model over baseline semi-supervised and fully-supervised models in varying proportions of labeled training data.

to segment the relevant anatomical structures. Our model leverages a large proportion of unlabeled data to learn to accomplish both tasks, which distinguishes it from existing methods where the semi-supervision applies to only one task in a multitask learning setting (Zhou et al., 2019).

Our specific contributions can be summarized as follows:

- A novel, general purpose, semi-supervised, multitask learning model leveraging self-supervision and adversarial training.
- The innovative use of chest and spine X-ray image data to tackle two important healthcare problems.
- Extensive experimentation showing the effectiveness of our model against state-of-the-art semi-supervised and fully-supervised single/multi-task models.

2. Related Work

We will now review the most relevant developments in computer vision and medical imaging in the field of semi-supervised learning and multitask learning.

2.1. Semi-Supervised Learning

Semi-supervised learning has recently been explored both in computer vision and medical imaging due to the availability of vast amounts of unlabeled data and computing power to process them. Semi-supervised learning is usually performed with a small portion of labeled and a larger portion of unlabeled data, assuming that both are from the same or similar distributions. In standard protocols, semi-supervised models are evaluated by retaining only a portion of the labels from a dataset while the remainder are treated as unlabeled data (Zhai et al., 2019). Depending on the

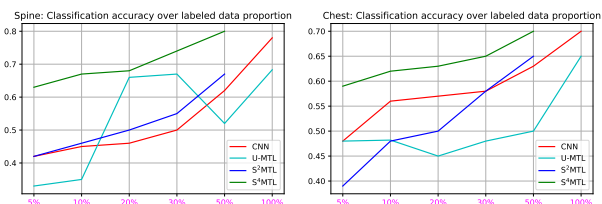


Figure 2. Consistent improvement in classification accuracy by the proposed S^4 MTL model over baseline semi-supervised and fully-supervised models in varying proportions of labeled training data.

approach to gaining information from large quantities of unlabeled data, semi-supervised learning can be performed in at least two different ways—self-supervised and adversarial training.

Self-supervised learning is similar to unsupervised learning in its goal of using a vast amount of unlabeled data to learn visual representation without any human annotation. Usually, self-supervised learning is performed by formulating a pretext or surrogate task only on the unsupervised data portion. Examples of pretext tasks could include image reconstruction, image colorization, predicting image rotations, etc. In self-supervision, data itself lends for supervision; i.e., proxy labels created from the data on which training can provide useful visual features from unlabeled data. Tajbakhsh et al. (2019) showed the effectiveness of training models from pre-trained surrogate tasks in different medical imaging applications, including diabetic retinopathy classification, nodule detection, and lung lobe segmentation with limited labeled data. Moreover, without training separately, both the pretext and downstream tasks can be combined in jointly learning useful visual features. Tran (2019) proposed a semi-supervised learning scheme based on self-supervision, where the model is trained like full-

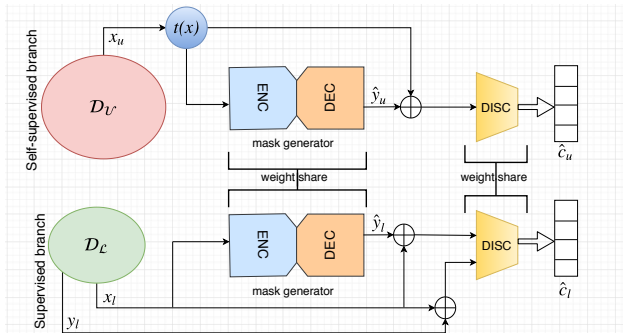


Figure 3. Schematic of the self-supervised, semi-supervised, multitask learning model (S^4 MTL). A segmentation mask generator produces masks on taking inputs from labeled or unlabeled samples. A class discriminator takes concatenated inputs from labeled data-mask or unlabeled data-mask pairs and predicts the class labels. For the labeled data branch, it is fully supervised. By contrast, using unlabeled data, the self-supervised branch employs self-generated labels using a geometric transformation function $t(x)$. The predicted segmentation output is obtained from the decoder (DEC) and the diagnostic classification prediction is received at the discriminator (DISC).

supervision—a supervised branch for the labeled data and a self-supervised branch for the unlabeled data—to predict some geometric transformations.

Adversarial learning can effectively be adapted to semi-supervised learning for classification of both natural and medical images (Salehinejad et al., 2018; Imran & Terzopoulos, 2019). Adversarial learning has also been utilized in segmentation (semantic-aware generative adversarial nets (Chen et al., 2018), structure correcting adversarial nets (Dai et al., 2018), etc.) as well as in disease classification (semi-supervised domain adaptation (Madani et al., 2018), attention-guided CNN (Guan et al., 2018)).

2.2. Multitask Learning

Multitask learning (MTL) can be accomplished in several ways, such as learning from auxiliary tasks to support the main task (Liebel & Körner, 2018), learning to learn multitask models (Zhang et al., 2018), joint learning of multiple tasks (Liu et al., 2019; Imran & Terzopoulos, 2019), etc. By performing multiple tasks, the domain-specific information in the training signals of related tasks is actually improved (Caruana, 1993). MTL is particularly useful for implicit data augmentation through better representation, focusing attention on the most relevant features, learning one task through another, and regularizing among them (Ruder, 2017).

The literature includes several efforts on performing multiple tasks within the same model. Several prior efforts address multitask learning with CNNs and generative modeling. Rezaei et al. (2018) combined a set of auto-encoders with an LSTM unit and an FCN as discriminator for seman-

tic segmentation and disease prediction. Girard et al. (2019) used a U-Net-like architecture coupled with graph propagation to jointly segment and classify retinal vessels. Mehta et al. (2018) proposed a Y-Net, with parallel discriminative and convolutional modularity, for the joint segmentation and classification of breast biopsy images. Another multitasking model was proposed by Yang et al. (2017) for skin lesion segmentation and melanoma-seborrheic keratosis classification, using GoogleNet extended to three branches for segmentation and two classification predictions. Khosravan & Bagci (2018) used a semi-supervised multitask model for the joint learning of false positive reduction and nodule segmentation from 3D computed tomography (CT) images. Most recently, Imran & Terzopoulos (2019) proposed an SSL model for the joint classification and segmentation of medical images in an adversarial training framework; however, no assumption was made on the distributions of labeled and unlabeled data and training was performed by simply masking out the labels for the unsupervised data.

As a departure from the existing SSL and MTL models, we propose the joint classification and segmentation of medical images via a novel SSL model with MTL leveraged by self-supervision and adversarial learning.

3. The S^4 MTL Model

We combine the concepts of self-supervision and adversarial learning in a semi-supervised multitask learning scheme for jointly performing image recognition and semantic segmentation within the same model. To formulate the problem, we assume an unknown data distribution $p(X, Y, C)$ over images, segmentation labels, and class labels. The model has access to the labeled training set \mathcal{D}_L sampled i.i.d. from $p(X, Y, C)$ and to the unlabeled training set \mathcal{D}_U sampled i.i.d. from $p(X)$ after marginalizing out Y and C . We set the learning objectives for both classification and segmentation tasks as

$$\min_{\psi, \theta} \mathcal{L}_L(\mathcal{D}_L, (\psi, \theta)) + \alpha \mathcal{L}_U(\mathcal{D}_U, (\psi, \theta)), \quad (1)$$

where the supervised loss \mathcal{L}_L is defined on the labeled data and the unsupervised loss \mathcal{L}_U is defined on the unlabeled data, α is a non-negative weight parameter, and ψ and θ denote the parameters of the classification and the segmentation networks, respectively.

Referring to Fig. 3, the S^4 MTL model comprises two main components—a segmentation mask generator G and a class discriminator D . Generator G can be any segmentation network, such as U-Net (Ronneberger et al., 2015), and any CNN classifier (LeCun et al., 2010) may be used as discriminator D . The model has a supervised branch for the labeled data and a self-supervision branch for the unlabeled data, and the two branches share the same G and D . Labeled data are passed through the supervised branch and supervised losses are calculated. Unsupervised losses are computed by

Algorithm 1 S⁴MTL Mini-Batch Training.

Require:

Training set of labeled data $x_l, y_l, c_l \in \mathcal{D}_L$
 Training set of unlabeled inputs $x_u \in \mathcal{D}_U$
 Transformation function $t(x)$ to generate c_u from x_u
 Network architecture $D_\psi, G_\theta \in \mathcal{F}_{(\psi, \theta)}$ with learnable parameters ψ, θ

for each epoch over \mathcal{D}_U **do**

Generate minibatches of unlabeled inputs \mathcal{M}_U using $t(x)$

for each step **do**

Sample minibatch $x_{l(i)}; x_{l(1)}, \dots, x_{l(m)} \sim \mathcal{P}_{\mathcal{D}_L}(x)$
 Sample minibatch $x_{u(i)}; x_{u(1)}, \dots, x_{u(m)} \sim \mathcal{P}_{\mathcal{D}_U}(x)$

Compute model outputs for the labeled inputs:

$$\hat{y}_l, \hat{c}_l \leftarrow \mathcal{F}_{(\psi, \theta)}(\mathcal{M}_L)$$

Compute model outputs for the unlabeled inputs:

$$\hat{y}_u, \hat{c}_u \leftarrow \mathcal{F}_{(\psi, \theta)}(\mathcal{M}_U)$$

Update the class discriminator D along its gradient:

$$\nabla_{\psi_D} \frac{1}{|\mathcal{M}_L|} \sum_{i \in \mathcal{M}_L} \left[L_D(x_{l(i)}, y_{l(i)}, \hat{y}_{l(i)}, c_{l(i)}, \hat{c}_{l(i)}) \right] + \alpha \frac{1}{|\mathcal{M}_U|} \sum_{i \in \mathcal{M}_U} \left[L_D(x_{u(i)}, \hat{y}_{u(i)}, \hat{c}_{u(i)}) \right]$$

Update the segmentation mask generator G along its gradient:

$$\nabla_{\theta_G} \frac{1}{|\mathcal{M}_L|} \sum_{i \in \mathcal{M}_L} \left[L_S(x_{l(i)}, y_{l(i)}, \hat{y}_{l(i)}) \right] + \alpha \frac{1}{|\mathcal{M}_U|} \sum_{i \in \mathcal{M}_U} \left[L_G(x_{u(i)}, \hat{y}_{u(i)}) \right]$$

end for
end for

feeding the unlabeled data through the unsupervised branch. The two networks G and D are trained in an adversarial learning manner, where the mask generator and the class discriminator compete against each other. The objective in (1) is therefore specified as two losses \mathcal{L}_D and \mathcal{L}_G for the two networks D and G , respectively:

$$\begin{aligned} \min_{\psi} \mathcal{L}_D(\mathcal{L}(\mathcal{D}_L, \psi_D) + \alpha \mathcal{L}(\mathcal{D}_U, \psi_D)), \\ \min_{\theta} \mathcal{L}_G(\mathcal{L}(\mathcal{D}_L, \theta_G) + \alpha \mathcal{L}(\mathcal{D}_U, \theta_G)). \end{aligned} \quad (2)$$

Algorithm 1 specifies the overall training procedure of the S⁴MTL model.

3.1. Self-Supervision

Self-supervision is usually formulated on two tasks—a surrogate or pretext task and a downstream or main task. Unlike fine-tuning on the downstream task using the pre-trained model from the pretext task, we combine them and refer to the combination as the *pre-stream* (i.e., *Pretext + downstream*) task for concurrently performing supervision and self-supervision. Although the self-supervision can be applied to both labeled and unlabeled data, we confine self-supervision only to the unlabeled data. We define pretext tasks for the unlabeled data \mathcal{D}_U . The self-supervision applies to the class discriminator D , whereas it is still unsupervised at the mask generator G . For the classification, we use a transformation function $t(x)$ to randomly flip (horizontal/vertical) or rotate (0, 90, 180, etc.) the unlabeled images and allow the network D predict them.

3.2. Classification

The real samples and labels to G are presented in the forward pass. In the backward pass, the feedback from D is passed to G . In the original image generator GAN, the discriminator works as a binary classifier, classifying the input image as real or synthetic. In order to facilitate the training of an n -class classifier, we expand the role of our class discriminator D to an $(n + 1)$ -classifier. For multiple logit generation, we replace the sigmoid function by a softmax function, such that it can receive concatenated image-mask (x_l, y_l) , image-predicted mask (x_l, \hat{y}_l) for labeled data, and (x_u, \hat{y}_u) for unlabeled data as inputs, and output an $(n + 1)$ -dimensional vector of logits $\{l_1, l_2, \dots, l_{n+1}\}$, which are finally transformed into class probabilities for the final classification. The class probabilities for the labeled data are calculated as

$$p(\hat{c}_l = (c_l = i) | (x_l, y_l)) = \frac{\exp(l_i)}{\sum_{j=1}^{n+1} \exp(l_j)} \quad (3)$$

and for the unlabeled data as

$$p(\hat{c}_u = (c_u = i) | (x_u, \hat{y}_u)) = \frac{\exp(l_i)}{\sum_{j=1}^{n+1} \exp(l_j)}. \quad (4)$$

3.3. Segmentation

The segmentation mask generator takes input x_l and generates \hat{y}_l for the labeled data. For the unlabeled data, mask prediction \hat{y}_u is generated from input x_u . For the labeled data, it is just like regular supervised segmentation. We employ Dice loss for the base model. Since the ground truth mask y_l is also available, the segmentation loss is calculated as

$$L_{G_{\mathcal{L}}(\text{seg})} = 1 -$$

$$\frac{\sum_i^{m^2} y_{pk}^{(i)} \hat{y}_{pk}^{(i)}}{\sum_i^{m^2} y_{pk}^{(i)} \hat{y}_{pk}^{(i)} + \frac{1}{2} \sum_i^{m^2} y_{pk}^{(i)} \hat{y}_{pk}^{(i)} + \frac{1}{2} \sum_i^{m^2} y_{pk}^{(i)} \hat{y}_{pk}^{(i)}}. \quad (5)$$

On the other hand, the ground truth mask for the unlabeled data is not available; therefore, we cannot directly calculate the segmentation loss on the predicted mask \hat{y}_u . Instead, we use an unsupervised loss—logit-wise distribution matching via KL divergence. The logit-wise absolute KL divergence (Imran & Terzopoulos, 2019) between the ground truth of labeled data y_l and prediction on unlabeled data \hat{y}_u over each pixel i and logit k is

$$L_{G_{\text{KL}}}(\mathcal{D}_U) = \sum_i^{m^2} |(y_{l_{pk}}(i) - \hat{y}_{u_{pk}}(i)) \log(y_{l_{pk}}(i)/\hat{y}_{u_{pk}}(i))|. \quad (6)$$

3.4. Final Losses

Depending on the source of the model inputs, G and D have multiple objectives for labeled and unlabeled data, combined for training with gradient descent.

Like any supervised learning model, G 's supervised loss is just based on the labeled samples (at pixel-level). We employ the generalized Dice loss in this regard. As in adversarial training, the generator's objective includes segmentation loss and adversarial prediction loss, where the segmentation mask generator G wants the class discriminator D to maximize the likelihood for the generated segmentation masks. For the labeled examples, we calculate two-way losses from image-label and image-prediction pairs, which differs from the unlabeled examples, where only image-prediction pairs are taken into account. The segmentation loss terms are calculated using (5)–(6). The unsupervised adversarial prediction loss terms include adversarial prediction losses for the labeled and unlabeled data. The mask generator G wants the class discriminator to maximize the likelihood for the image-prediction pairs x_l, \hat{y}_l . Therefore, the adversarial prediction loss in G is

$$L_{G_{\text{pred}}(x_l, \hat{y}_l)} = -\mathbb{E}_{x_l, \hat{y}_l \sim G} \log[1 - p(c_l = n + 1 | (x_l, \hat{y}_l))]. \quad (7)$$

Similarly, for the unlabeled data, x_u, \hat{y}_u , the adversarial prediction loss is

$$L_{G_{\text{pred}}(x_u, \hat{y}_u)} = -\mathbb{E}_{x_u, \hat{y}_u \sim G} \log[1 - p(c_u = n + 1 | (x_u, \hat{y}_u))]. \quad (8)$$

Since the main objective of G is to generate the segmentation map, a small weight is used for the adversarial loss terms for both labeled and unlabeled data.

The class discriminator D is trained on multiple objectives—adversary on the segmentation mask generator G 's output and classification of the images into the real or surrogate classes. Since the model is trained on both labeled and unlabeled training data, the loss function L_D of the class discriminator D includes both supervised and unsupervised losses. Function L_D includes five different loss terms: 1) supervised classification loss on $(\hat{c}_l | x_l, y_l)$, 2) self-supervised

classification loss on unlabeled data $(\hat{c}_u | x_u, \hat{y}_u)$, 3) adversarial real loss on x_l, y_l , 4) adversarial prediction loss on x_l, \hat{y}_l , and 5) adversarial prediction loss on x_u, \hat{y}_u . The supervised losses are calculated as

$$L_{D_{\text{sup}}} = -\mathbb{E}_{x_l, y_l, c_l \sim p_{\mathcal{D}_L}} \log[p(\hat{c}_l = (c_l = i) | x_l, y_l; i < n + 1)] \quad (9)$$

and

$$L_{D_{\text{self}}} = -\mathbb{E}_{x_u, \hat{y}_u, c_u \sim p_{\mathcal{D}_U}} \log[p(\hat{c}_u = (c_u = i) | x_u, \hat{y}_u; i < n + 1)]. \quad (10)$$

Now, for the labeled data \mathcal{D}_L , D can receive two-way inputs (x_l, y_l) or (x_l, \hat{y}_l) . Therefore, the adversarial losses for \mathcal{D}_L are

$$L_{D_{\text{gt}}(\mathcal{D}_L)} = -\mathbb{E}_{x_l, y_l \sim p(\mathcal{D}_L)} \log[1 - p(c_l = n + 1 | x_l, y_l)] \quad (11)$$

and

$$L_{D_{\text{pred}}(\mathcal{D}_L)} = -\mathbb{E}_{(x_l, \hat{y}_l) \sim S} \log[p(c_l = n + 1 | x_l, \hat{y}_l)]. \quad (12)$$

For the unlabeled data \mathcal{D}_U , we calculate only the adversarial prediction loss

$$L_{D_{\text{pred}}(\mathcal{D}_U)} = -\mathbb{E}_{(x_u, \hat{y}_u) \sim S} \log[p(c_u = n + 1 | x_u, \hat{y}_u)]. \quad (13)$$

4. Experimental Evaluation

4.1. Datasets

We evaluate our S⁴MTL model against the baseline models using the following two datasets:

1. **Chest Dataset:** For our experiments, we make use of the Montgomery County chest X-ray set, the Shenzhen chest X-ray set available from the NIH (Jaeger et al., 2014), and the dataset available from the Japanese Society of Radiological Technology (JCX) (Shiraishi et al., 2000). Combining these three publicly available datasets, we create a dataset of 912 chest X-ray images, which we call the ‘‘Chest Dataset’’. We split it into three sets—training (615), validation (69), and test (228). Along with lung segmentation, we perform 3-class classification—normal, tuberculosis (TB), and nodule.
2. **Spine Dataset:** A dataset of 100 very high-resolution spinal X-ray images is obtained from a vertebral compression fracture study of osteoporosis (Wong & McGirt, 2013). The dataset contains pixel-wise annotation and binary disease label (normal and abnormal) for each of the vertebrae in lateral views. We extract extended patches from each individual vertebra and create a dataset of 994 patch images, which we call the

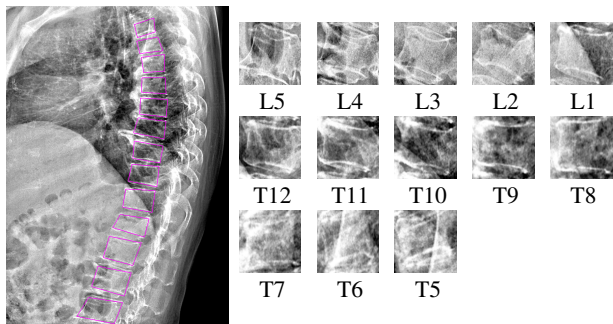


Figure 4. Individual vertebra patches along with their labels (vertebra indices) extracted from the lateral X-ray image. L: Lumbar vertebra, T: Thoracic vertebra. L5 is the bottom most vertebra; other vertebrae are shown in reverse order. In this X-ray image, only L2 is labeled osteoporosis positive (abnormal) while the remaining vertebrae are normal.

“Spine Dataset”. Fig. 4 demonstrates the extraction of vertebra patches from a spine X-ray image. The dataset was split into three subsets: train (713), validation (42), and test (139). We perform vertebra segmentation and abnormality prediction on each vertebra patch (normal vs abnormal).

For each dataset, we train the models on its training set (labeled and unlabeled data), use its validation set to determine the hyper-parameters and for model selection, and evaluate the models on its test set.

4.2. Implementation Details

Inputs: All the images are normalized and resized to $128 \times 128 \times 1$ before feeding them to the models.

Model Architecture: As the segmentation mask generator we use a U-Net like encoder-decoder network with skip connections, and as the class discriminator we used another convolutional network (Conv-Net) (Imran & Terzopoulos, 2019). We implement the S⁴MTL algorithm in Tensorflow running on a Tesla P40 GPU and a 64-bit Intel(R) Xeon(R) 440G CPU.

Baselines: As baselines, we use the segmentation mask generator (U-Net) and class discriminator (Conv-Net) networks separately for single-task models both in supervised and partially-supervised manners. Using the same backbone network, we also train a multitasking U-Net with a classification branch from its bottleneck layer (similarly as Y-Net (Mehta et al., 2018)), namely U-MTL. In addition, we experiment with another semi-supervised multitasking model without self-supervision and unsupervised segmentation losses. We call this the semi-supervised multitask learning (S²MTL) model.

Training: Following our formulated problem, \mathcal{D}_L and \mathcal{D}_U are selected before training the models, rather than just

masking some data out during training. We constrain all the semi-supervised models to having maximum 50% labeled data in order to hold $|\mathcal{D}_L| \leq |\mathcal{D}_U|$. The semi-supervised models (single-task or multitask) are trained on varying proportions of labeled data: 5%, 10%, 20%, 30%, and 50%. For example, when 10% is selected, 10% of the training data are used with their corresponding class and segmentation labels, and 90% are used without any label information. We adapt the training signal annealing in our model using the logarithmic schedule (Xie et al., 2019) with an adjustment for balancing between epochs and mini-batches. In our experiments, the signal annealing threshold $\eta_{(e,s)}$ is set to $1 - \exp(-\frac{s * e + 1}{E * N}) * (1 - \frac{1}{n}) + \frac{1}{n}$, where s is the current step, e is the current epoch, E is total number of epochs, N is the training dataset size, and n is the number of classes. In training, the labeled data are selected such that every class has equal representation in the training data \mathcal{D}_L . In the mask generator network, we use instance-normalization and ReLU activation. A dropout rate of 0.4 is applied after every convolutional layer.

Hyper-parameters: We use the Adam optimizer with adaptive learning rates for G and D . With initial learning rates $2e - 3$ with momentum 0.9 for G and $1e - 4$ with momentum 0.6 for D . The learning rates are adapted with exponential decay scheduled after every 2 epoch with decay rates of 0.9 and 0.5, respectively. Each model is trained with a mini-batch size of 16.

Evaluation: For classification, along with the overall accuracy, we record the class-wise F1 scores. Dice similarity (DS), average Hausdorff distance (HD), Jaccard index (JI), structural similarity measure (SSIM), precision (Prec), and recall (Rec) scores are used to evaluate the segmentation performance.

4.3. Results & Discussion

Classification: We validate our S⁴MTL model on two separate datasets and the performance evaluations are compared against semi-supervised and fully-supervised models. The consistent improvement of S⁴MTL with varying labeled data proportions is evident in Fig. 2. For both the Spine and Chest datasets, our S⁴MTL model is found to be superior to all the baseline models. Table 1 compares the classification performances among all the models, and our model achieves better overall and class-wise accuracies for both datasets, even better than the fully-supervised single-task and multi-task models.

Segmentation: The segmentation performance is evaluated both qualitatively and quantitatively. As shown in Table 2 and Table 3, our S⁴MTL model achieves the best scores compared to the semi-supervised, fully-supervised, single-task, and multitask models. The robustness of our S⁴MTL model is confirmed by its consistent performance for different proportions of labeled data (Fig. 1). Visualization

Table 1. Classification performance comparison of the S⁴MTL model against the baseline models in different data settings with varying proportions of labeled data.

Type	Model	Spine			Chest			
		Accuracy	F1(Normal)	F1(Abnormal)	Accuracy	F1(Normal)	F1(TB)	F1(Nodule)
Single-Task	Conv-Net-100%	0.780	0.740	0.800	0.700	0.530	0.720	0.840
	Conv-Net-50%	0.620	0.680	0.580	0.630	0.460	0.710	0.730
	Conv-Net-30%	0.500	0.000	0.630	0.580	0.590	0.360	0.710
	Conv-Net-20%	0.460	0.460	0.460	0.570	0.620	0.250	0.730
	Conv-Net-10%	0.450	0.490	0.410	0.560	0.630	0.180	0.710
	Conv-Net-5%	0.420	0.330	0.490	0.480	0.650	0.000	0.000
Multitask	UMTL-100%	0.683	0.810	0.008	0.650	0.610	0.290	0.780
	UMTL-50%	0.520	0.580	0.430	0.500	0.680	0.200	0.000
	UMTL-30%	0.670	0.800	0.000	0.480	0.650	0.000	0.000
	UMTL-20%	0.660	0.800	0.000	0.450	0.530	0.450	0.000
	UMTL-10%	0.350	0.030	0.051	0.482	0.650	0.000	0.000
	UMTL-5%	0.331	0.000	0.050	0.480	0.650	0.000	0.000
	S ² MTL-50%	0.670	0.800	0.000	0.650	0.610	0.290	0.780
	S ² MTL-30%	0.550	0.680	0.250	0.580	0.590	0.380	0.690
	S ² MTL-20%	0.500	0.000	0.630	0.500	0.570	0.410	0.490
	S ² MTL-10%	0.460	0.430	0.490	0.480	0.650	0.000	0.000
	S ² MTL-5%	0.420	0.330	0.500	0.390	0.470	0.350	0.280
	S ⁴ MTL-50%	0.800	0.790	0.810	0.700	0.530	0.710	0.730
	S ⁴ MTL-30%	0.740	0.810	0.700	0.650	0.780	0.310	0.400
	S ⁴ MTL-20%	0.680	0.790	0.290	0.630	0.630	0.290	0.410
S ⁴ MTL-10%	0.670	0.800	0.000	0.620	0.620	0.300	0.840	
S ⁴ MTL-5%	0.630	0.730	0.410	0.590	0.600	0.360	0.710	

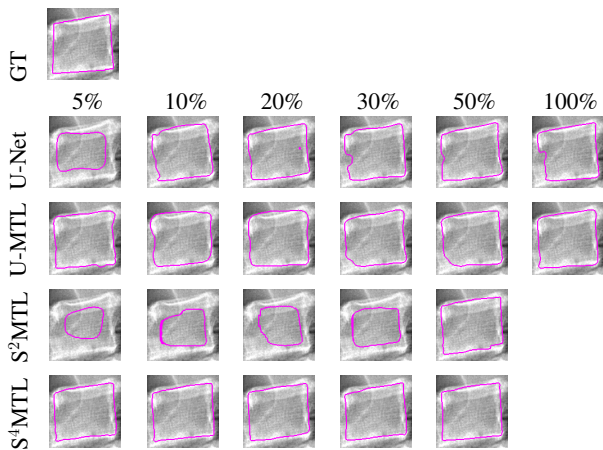


Figure 5. Spine Dataset: Boundary visualization of a predicted vertebra mask showing the superiority of our S⁴MTL model over the baseline models with varying proportions of labeled data.

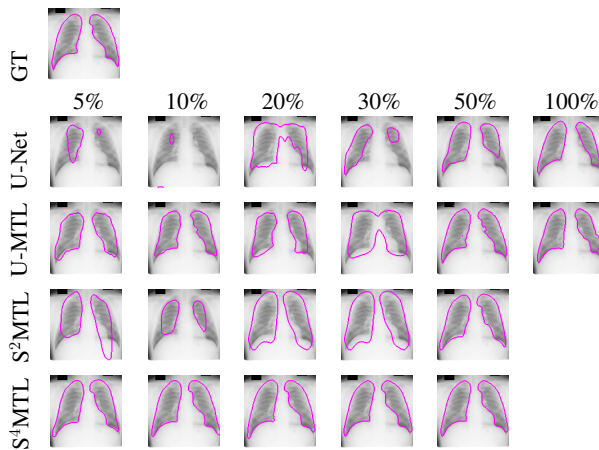


Figure 6. Chest Dataset: Boundary visualization of the predicted lung masks in a chest X-Ray shows consistent improvement with our S⁴MTL model against the semi-supervised and fully-supervised baselines with varying proportions of labeled data.

of the segmented vertebra and lung boundaries by different models in varying labeled data proportions (Fig. 5 and Fig. 6) confirms the effectiveness of our model over competing models. For a fair comparison of all the models, a common segmentation backbone is used in the single-task for segmentation and in the multitask for segmentation mask generator. Our S⁴MTL model consistently performs better than the semi/fully-supervised single-task (U-Net) and multitask (U-MTL) models, given the same number of labeled data during training ($|\mathcal{D}_L|$). The advantage really comes with the knowledge gain from the larger proportion of unlabeled data and multitask learning, S⁴MTL’s forte. This

clearly reveals the effectiveness of our model.

Statistical Analysis: To verify the significance of our model, we perform three different statistical tests, namely one-way ANOVA, paired-t, and Wilcoxon signed-rank tests. All three tests confirm that our S⁴MTL model with 50% labeled data model shows significant improvement over all the semi-supervised and fully-supervised baselines in the Chest Dataset (p-value < 0.05). Moreover, for the Spine Dataset, our S⁴MTL model with 50% labeled data is found to be significantly different from all the baseline models except the fully-supervised U-Net model. The Bland-Altman

Table 2. Spine performance: Vertebra segmentation comparison of the S⁴MTL model against the baselines for supervised/semi-supervised single-task and multitasking in different data settings with varying proportion of labeled data.

Dataset	Type	Model	DS	JI	SSIM	HD	Prec	Rec
Spine	Single-Task	U-Net-100%	0.931	0.872	0.874	4.335	0.954	0.911
		U-Net-50%	0.919	0.851	0.857	4.569	0.949	0.893
		U-Net-30%	0.910	0.835	0.847	4.836	0.946	0.877
		U-Net-20%	0.903	0.824	0.839	5.022	0.935	0.873
		U-Net-10%	0.874	0.776	0.801	5.276	0.923	0.830
		U-Net-5%	0.702	0.541	0.685	6.909	0.957	0.554
	Multitask	U-MTL-100%	0.888	0.799	0.817	5.348	0.908	0.869
		U-MTL-50%	0.890	0.802	0.827	5.429	0.936	0.849
		U-MTL-30%	0.881	0.787	0.817	5.421	0.950	0.821
		U-MTL-20%	0.862	0.758	0.792	5.733	0.902	0.826
		U-MTL-10%	0.873	0.775	0.804	6.396	0.884	0.863
		U-MTL-5%	0.856	0.333	0.584	7.018	0.999	0.333
		S ² MTL-50%	0.889	0.801	0.821	4.956	0.887	0.893
		S ² MTL-30%	0.752	0.603	0.719	6.032	0.997	0.603
		S ² MTL-20%	0.672	0.506	0.670	6.256	0.998	0.506
		S ² MTL-10%	0.640	0.471	0.654	6.772	0.998	0.471
		S ² MTL-5%	0.500	0.333	0.584	7.018	0.999	0.333
		S ⁴ MTL-50%	0.934	0.876	0.875	3.762	0.947	0.921
S ⁴ MTL-30%	0.925	0.861	0.866	3.912	0.946	0.905		
S ⁴ MTL-20%	0.921	0.853	0.860	4.162	0.942	0.900		
S ⁴ MTL-10%	0.907	0.830	0.842	4.723	0.914	0.901		
S ⁴ MTL-5%	0.890	0.802	0.821	4.835	0.887	0.893		

plots shown in Fig. 7 also suggest good agreement between ground truth and the prediction by our S⁴MTL model for both datasets. Moreover, we perform a robustness analysis to compare the class-wise segmentation performance of our S⁴MTL model. Fig. 8 shows that there are no significant differences among the class-wise segmentation performances (Dice scores). Furthermore, by performing one-way ANOVA, independent sample t-test, and Pearson correlation, we confirm that our model is robust against different disease classes (normal vs abnormal in the Spine dataset and normal vs TB vs nodule in the Chest dataset).

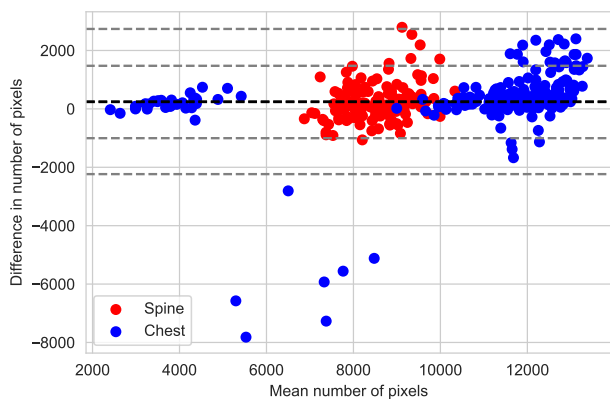


Figure 7. Bland-Altman plots show good agreement between the number of ground truth pixels and model (S⁴MTL-50%) predicted pixels for the test sets.

Table 3. Chest performance: Lung segmentation comparison of the S⁴MTL model against the baselines for semi-supervised multitasking in different data settings with varying proportion of labeled data.

Dataset	Type	Model	DS	JI	SSIM	HD	Prec	Rec
Chest	Single-Task	U-Net-100%	0.922	0.856	0.816	4.524	0.909	0.936
		U-Net-50%	0.892	0.806	0.761	5.382	0.846	0.945
		U-Net-30%	0.834	0.715	0.654	6.584	0.723	0.986
		U-Net-20%	0.815	0.688	0.636	5.979	0.758	0.882
		U-Net-10%	0.800	0.667	0.599	7.111	0.682	0.969
		U-Net-5%	0.788	0.650	0.583	7.419	0.654	0.991
	Multitask	U-MTL-100%	0.874	0.776	0.747	4.969	0.800	0.963
		U-MTL-50%	0.888	0.799	0.756	4.700	0.822	0.965
		U-MTL-30%	0.820	0.694	0.658	5.374	0.766	0.881
		U-MTL-20%	0.829	0.708	0.654	6.483	0.719	0.979
		U-MTL-10%	0.841	0.726	0.683	5.554	0.746	0.964
		U-MTL-5%	0.820	0.695	0.644	5.648	0.748	0.908
		S ² MTL-50%	0.810	0.681	0.636	4.862	0.782	0.840
		S ² MTL-30%	0.572	0.401	0.465	5.416	0.824	0.438
		S ² MTL-20%	0.607	0.436	0.516	5.782	0.987	0.438
		S ² MTL-10%	0.558	0.387	0.487	5.827	0.998	0.387
		S ² MTL-5%	0.458	0.300	0.421	7.496	0.989	0.300
		S ⁴ MTL-50%	0.946	0.898	0.864	3.432	0.964	0.939
S ⁴ MTL-30%	0.903	0.823	0.798	3.963	0.885	0.921		
S ⁴ MTL-20%	0.895	0.810	0.784	4.119	0.878	0.912		
S ⁴ MTL-10%	0.868	0.768	0.742	4.272	0.834	0.905		
S ⁴ MTL-5%	0.845	0.732	0.703	4.619	0.811	0.883		

5. Conclusions

Learning from small labeled datasets has been one of the most challenging tasks in computer vision and medical imaging. We have proposed a novel self-supervised, semi-supervised, multitask learning (S⁴MTL) model and validated it in medical image classification and segmentation experiments with limited labeled data. The effectiveness of our S⁴MTL model over semi-supervised and fully-supervised single-task and multitask models is confirmed by the experimental results. Moreover, S⁴MTL with 50% labeled data achieves better performance, with statistical significance, over all other semi-supervised models.

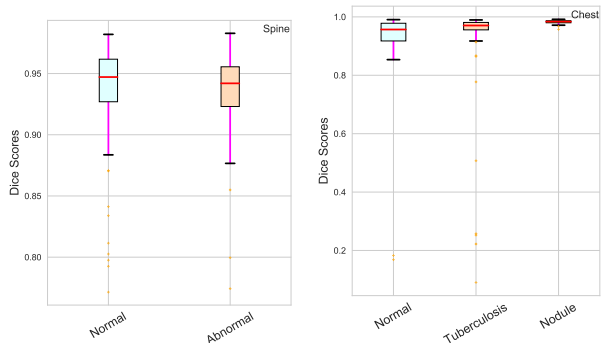


Figure 8. Class-wise boxplots showing the robustness of our S⁴MTL-50% model in segmenting vertebrae and lungs from spinal and chest X-Rays.

Our model may further, be utilized in general settings when data available with and without labels have dissimilar distributions. A worthwhile next step would be experimenting with more sophisticated medical imaging and computer vision data at larger scale and in more challenging settings.

References

- Caruana, R. A. Multitask learning: A knowledge-based source of inductive bias. In *International Conf. on Machine Learning*, pp. 41–48, 1993.
- Chapelle, O., Scholkopf, B., and Zien, A. Semi-supervised learning. *IEEE Transactions on Neural Networks*, 20(3): 542–542, 2009.
- Chen, C., Dou, Q., Chen, H., and Heng, P.-A. Semantic-aware generative adversarial nets for unsupervised domain adaptation in chest X-ray segmentation. In *International Workshop on Machine Learning in Medical Imaging*, pp. 143–151. Springer, 2018.
- Dai, W., Dong, N., Wang, Z., Liang, X., Zhang, H., and Xing, E. P. SCAN: Structure correcting adversarial network for organ segmentation in chest X-rays. In *Deep Learning in Medical Image Analysis*, volume 11045 of LNCS. 2018.
- Donahue, J., Krähenbühl, P., and Darrell, T. Adversarial feature learning. *arXiv preprint arXiv:1605.09782*, 2016.
- Girard, F., Kavalec, C., and Cheriet, F. Joint segmentation and classification of retinal arteries/veins from fundus images. *Artificial Intelligence in Medicine*, 94:96–109, 2019.
- Goodfellow, I., Pouget-Abadie, J., Mirza, M., Xu, B., Warde-Farley, D., Ozair, S., Courville, A., and Bengio, Y. Generative adversarial nets. In *Advances in Neural Information Processing Systems*, pp. 2672–2680, 2014.
- Guan, Q., Huang, Y., Zhong, Z., Zheng, Z., Zheng, L., and Yang, Y. Diagnose like a radiologist: Attention guided convolutional neural network for thorax disease classification. *arXiv preprint arXiv:1801.09927*, 2018.
- Imran, A.-A.-Z. and Terzopoulos, D. Multi-adversarial variational autoencoder networks. In *2019 18th IEEE International Conference On Machine Learning And Applications (ICMLA)*, pp. 777–782, 2019.
- Imran, A.-A.-Z. and Terzopoulos, D. Semi-supervised multi-task learning with chest X-ray images. In *Machine Learning in Medical Imaging*, volume 11861 of *Lecture Notes in Computer Science*, pp. 151–159. Springer, 2019.
- Jaeger, S., Candemir, S., Antani, S., Wang, Y.-X. J., Lu, P.-X., and Thoma, G. Two public chest X-ray datasets for computer-aided screening of pulmonary diseases. *Quantitative imaging in medicine and surgery*, 4(6):475, 2014.
- Jing, L. and Tian, Y. Self-supervised visual feature learning with deep neural networks: A survey. *arXiv preprint arXiv:1902.06162*, 2019.
- Khosravan, N. and Bagci, U. Semi-supervised multi-task learning for lung cancer diagnosis. In *2018 40th Annual International Conference of the IEEE Engineering in Medicine and Biology Society (EMBC)*, pp. 710–713. IEEE, 2018.
- LeCun, Y., Kavukcuoglu, K., Farabet, C., et al. Convolutional networks and applications in vision. In *International Symposium on Circuits and Systems (ISCAS’10)*, 2010.
- Liebel, L. and Körner, M. Auxiliary tasks in multi-task learning. *arXiv preprint arXiv:1805.06334*, 2018.
- Liu, X., Sukanuma, M., and Okatani, T. Joint learning of multiple image restoration tasks. *arXiv preprint arXiv:1907.04508*, 2019.
- Madani, A., Moradi, M., Karagyris, A., and Syeda-Mahmood, T. Semi-supervised learning with generative adversarial networks for chest X-ray classification with ability of data domain adaptation. In *Proc. ISBI*, pp. 1038–1042, 2018.
- Mehta, S., Mercan, E., Bartlett, J., et al. Y-Net: Joint segmentation and classification for diagnosis of breast biopsy images. In *MICCAI*, 2018.
- Rezaei, M., Yang, H., et al. Multi-task generative adversarial network for handling imbalanced clinical data. *CoRR*, 2018.
- Ronneberger, O., Fischer, P., and Brox, T. U-net: Convolutional networks for biomedical image segmentation. In *Proc MICCAI*, pp. 234–241. Springer, 2015.
- Ruder, S. An overview of multi-task learning in deep neural networks. *arXiv preprint arXiv:1706.05098*, 2017.
- Salehinejad, H., Valaee, S., Dowdell, T., Colak, E., and Barfett, J. Generalization of deep neural networks for chest pathology classification in X-rays using generative adversarial networks. In *ICASSP*, 2018.
- Shiraishi, J., Katsuragawa, S., et al. Development of a digital image database for chest radiographs with and without a lung nodule. *J of Roent*, 2000.
- Tajbakhsh, N., Hu, Y., Cao, J., Yan, X., Xiao, Y., Lu, Y., Liang, J., Terzopoulos, D., and Ding, X. Surrogate supervision for medical image analysis: Effective deep learning from limited quantities of labeled data. In *Proc. IEEE International Symposium on Biomedical Imaging (ISBI’19)*, pp. 1251–1255, 2019.

- Tran, P. V. Semi-supervised learning with self-supervised networks. *arXiv preprint arXiv:1906.10343*, 2019.
- Wong, C. C. and McGirt, M. J. Vertebral compression fractures: a review of current management and multimodal therapy. *Journal of Multidisciplinary Healthcare*, 6:205, 2013.
- Xie, Q., Dai, Z., Hovy, E., Luong, M.-T., and Le, Q. V. Unsupervised data augmentation. *arXiv preprint arXiv:1904.12848*, 2019.
- Yang, J., Dvornek, N. C., Zhang, F., Zhuang, J., Chapiro, J., Lin, M., and Duncan, J. S. Domain-agnostic learning with anatomy-consistent embedding for cross-modality liver segmentation. In *Proceedings of the IEEE International Conference on Computer Vision Workshops*, 2019.
- Yang, X., Zeng, Z., Yeo, S. Y., et al. A novel multi-task deep learning model for skin lesion segmentation and classification. *arXiv:1703.01025*, 2017.
- Zhai, X., Oliver, A., Kolesnikov, A., and Beyer, L. S⁴I: Self-supervised semi-supervised learning. *arXiv preprint arXiv:1905.03670*, 2019.
- Zhang, Y. and Yang, Q. A survey on multi-task learning. *arXiv preprint arXiv:1707.08114*, 2017.
- Zhang, Y., Wei, Y., and Yang, Q. Learning to multitask. In *Advances in Neural Information Processing Systems*, pp. 5771–5782, 2018.
- Zhang, Y., Liu, T., Long, M., and Jordan, M. I. Bridging theory and algorithm for domain adaptation. *arXiv preprint arXiv:1904.05801*, 2019.
- Zhou, Y., He, X., Huang, L., Liu, L., Zhu, F., Cui, S., and Shao, L. Collaborative learning of semi-supervised segmentation and classification for medical images. In *Proc CVPR*, pp. 2079–2088, 2019.
- Zhuang, F., Qi, Z., Duan, K., Xi, D., Zhu, Y., Zhu, H., Xiong, H., and He, Q. A comprehensive survey on transfer learning. *arXiv preprint arXiv:1911.02685*, 2019.